Journal of ELECTRONIC MATERIALS, Vol. 46, No. 4, 2017
DOI: 10.1007/s11664-017-5291-5

Growth and Characterization of Sn Doped β-Ga_2O_3 Thin Films and Enhanced Performance in a Solar-Blind Photodetector

XIAOLONG ZHAO,[1] WEI CUI,[1] ZHENPING WU,[1] DAOYOU GUO,[1] PEIGANG LI,[1] YUEHUA AN,[1] LINGHONG LI,[2] and WEIHUA TANG[1,3]

1.—Laboratory of Optoelectronics Materials and Devices, School of Science, Beijing University of Posts and Telecommunications, Beijing 100876, China. 2.—Department of Physics, The State University of New York at Potsdam, Potsdam, NY 13676-2294, USA. 3.—e-mail: whtang@bupt.edu.cn

$Ga_{2-x}Sn_xO_3$ thin films were deposited on c-plane Al_2O_3 (0001) substrates with different Sn content by laser molecular beam epitaxy technology (L-MBE). The Sn content x was varied from 0 to 1.0. ($\bar{2}01$) oriented β-phase $Ga_{2-x}Sn_xO_3$ thin films were obtained at the substrate temperature of 850°C in the vacuum pressure of 5×10^{-5} Pa. The crystal lattice expanded and the energy band-gap decreased with the increase of Sn content for Sn^{4+} ions incorporated into the Ga site. The n-type conductivity was generated effectively through doping Sn^{4+} ions in the Ga_2O_3 lattice in the oxygen-poor conditions. The solar-blind (SB) photodetectors (PDs) based on $Ga_{2-x}Sn_xO_3$ (x = 0, 0.2) thin films were fabricated. The current intensity and responsivity almost increased by one order of magnitude and the relaxation time constants became shorter for x = 0.2. Our work suggests that the performance of PD can be improved by doping Sn^{4+} ions in Ga_2O_3 thin films.

Key words: Ga_2O_3, thin film, Sn-doped, solar-blind, photodetector

INTRODUCTION

The terrestrial ozone layer has a strong absorption for ultraviolet (UV) radiation (200–280 nm) from the solar light radiation through the atmosphere; this waveband of UV radiation nearly does not exist both at the surface of the earth and in the atmosphere near sea level, the so-called SB region.[1,2] The PD produces that accordingly by operating in the SB region and is named the solar-blind photodetector (SBPD). The SBPD is used in many fields, for instance, fire detection, missile tracking, electrical arcing, chemical-biological analysis, and so forth.[3] At present, the transparent semiconducting oxides (TSOs) have been applied in the field of SBPD. The TSOs constitute a kind of material that combines almost 90% visible-light transparency with electrical conductivity.[4] Due to a small energy band-gap (~3.2 eV), the conventional TSOs such as ZnO, SnO_2 and In_2O_3 are opaque in the UV region ($\lambda <$ 300 nm). With the improvement of the epitaxial growth and the process techniques, the wide band-gap semiconductors are applied in SBPDs, for instance, AlGaN, diamond and ZnMgO. Although AlGaN alloys have a high Al content to serve as the active light absorption layer, the quality of the epitaxial layer deteriorates rapidly with increasing Al content.[5] Meanwhile, the photocurrent sensitivity of the diamond is restricted to the wavelengths below 225 nm because of the band-gap energy (E_g) is 5.5 eV.[6] In addition, it is difficult to grow the single ZnMgO with high Mg content because of the phase segregation that occurs in both ZnO and MgO.[7] Thus, new TSOs materials need to be explored so as to increase the performance of SBPD.

Ga_2O_3 has recently attracted increasing interest as a kind of TSO, which occurs in various phases like α-, β-, γ-, δ-, and ε-phase.[8] Among them, β-phase Ga_2O_3 is considered to be in common use with it being the most stable thermally and chemically.[9] Its melting point (~1740°C) determines the possibility of working at a high

(Received April 27, 2016; accepted January 5, 2017; published online February 2, 2017)

temperature.[10] The β-phase Ga_2O_3 single crystal belongs to the monoclinic system with space group $C2/m$, in which Ga^{3+} ions occupy both tetrahedral and octahedral sites, and the lattice parameters are a = 12.23 Å, b = 3.04 Å, c = 5.08 Å, β = 103.83°, respectively.[11,12] It is an indispensable material for SBPD because of the band-gap energy of β-phase Ga_2O_3 is 4.9 eV.[13] In fact, pure β-phase Ga_2O_3 thin film has been demonstrated in SBPD.[14,15] So far, the fabrication of high performance PD using β-Ga_2O_3 thin film is still challenge. There are some factors affecting the performance of PD based on β-Ga_2O_3 thin film, for instance, quality of films, interface of metal-electrode/semiconductor,[16] structure of electrodes, and defects and doping. Both defects and doping affect the conductivity of thin films significantly, which makes it one of the most basic factors for increasing the performance of PD.[17] It is found that the undoped Ga_2O_3 thin films are of n-type conductivity as they grow in lower oxygen partial pressure.[18] The oxygen vacancies have been regarded as the origin of intrinsic n-type conductivity,[19] and the conductivity up to 1 S cm^{-1} was obtain by Orita under low oxygen partial pressure.[20] The density of the oxygen vacancies is strongly dependent on the deposition temperature during the deposition process. The opto-electronic properties, including E_g, electron affinity and charge carrier density are found to be influenced by the oxygen vacancies.[21] Recent research found that a shallow donor level was achieved by doping Sn^{4+} ions in Ga_2O_3 thin films. The conductivity of Sn-doped Ga_2O_3 thin films decreased with the Sn content change in a certain range.[22–24] We set a low oxygen partial pressure of ambient atmosphere and a high substrate temperature, which could enlarge the chemical potential of oxygen in the lattice resulting in the formation of oxygen defects and Sn^{4+} ions into the lattice effectively at a high substrate temperature by releasing oxygen gas into the atmosphere.

At present, Sn-doped β-phase Ga_2O_3 thin films have been prepared by many methods, such as metal organic chemical vapor deposition,[22–24] pulsed laser deposition,[20] radio frequency magnetron sputtering (RFMS),[25] and so on. Compared to these methods, L-MBE possesses a closed vacuum system to insure high-purity source materials and a pollution-free environment. Moreover, the atomic-layer growth can be monitored by in situ reflection high energy electron diffraction (RHEED) so that fabrication of the films with high crystal quality for more excellent device properties can occur.[26] In this work, we prepared β-phase $Ga_{2-x}Sn_xO_3$ thin films on Al_2O_3 (0001) substrates with different Sn content by L-MBE. Meanwhile, a prototype device of SBPD with metal–semiconductor-metal (MSM) structure based on β-phase $Ga_{2-x}Sn_xO_3$ (x = 0, 0.2) thin films was fabricated and compared with the UV photoresponse of two SBPDs.

EXPERIMENTAL

The Sn-doped Ga_2O_3 target was prepared from Ga_2O_3 (purity, 5 N) and SnO_2 (purity, 5 N) powders. The Ga_2O_3 and SnO_2 powders were thoroughly mixed on the basis of the composition ratio x (x = 0, 0.2, 0.6, 1.0), pressed into a disk, and then sintered. A substrate of c-plane Al_2O_3 (0001) single crystal was put in the deposition chamber and the vacuum pressure in the chamber was 5×10^{-5} Pa. The $Ga_{2-x}Sn_xO_3$ (x = 0, 0.2, 0.6, 1.0) sintered body was irradiated by focused KrF excimer laser beam with a wavelength of 248 nm. The laser pulse energy density was 4 J/$cm^{2,}$ and the target-substrate distance was 50 mm. The substrate was rotated in order to improve the film's uniformity during the deposition process. The structural properties of β-phase $Ga_{2-x}Sn_xO_3$ thin films were characterized by a Hitachi S-4800 field emission scanning electron microscope (FE-SEM) operating at 10 keV. An energy dispersive x-ray (EDX) spectrum of the samples was also measured. The crystallinity and orientation of the as-grown films were investigated by x-ray diffraction (XRD) at θ-2θ scan using a PANalytical X'pert PRO diffractometer with Cu Ka (λ = 1.5405 Å) radiation and in situ RHEED. An ultraviolet–visible (UV–vis) absorption spectrum was recorded using a Hitachi U-3900 UV–vis spectrophotometer. For the fabrication of SBPD, the interdigital Au/Ti electrode was deposited on the thin film surface using a shadow mask by a RFMS system. The size of the interdigitated electrode was 2.8 mm long, 0.2 mm wide, and the finger spacing was 0.2 mm. The current–voltage (I-V) and time-dependent photoresponse of β-phase $Ga_{2-x}Sn_xO_3$ PD were measured by a Keithley 2450 system. An UV lamp served as the light source with a wavelength of 254 nm and the effective irradiated area of PD was 0.045 cm^2.

RESULTS AND DISCUSSION

Figure 1a exhibits XRD patterns of $Ga_{2-x}Sn_xO_3$ thin films deposited on Al_2O_3 (0001) substrates with different Sn content at the substrate temperature of 850°C in vacuum pressure of 5×10^{-5} Pa. It is observed that the diffraction peaks are located at around 19°, 38°, and 59° except for the diffraction peaks of Al_2O_3 substrates. According to the powder diffraction file, all of them belong to $Ga_{2-x}Sn_xO_3$ and no peaks come from Sn metal clusters, Sn oxide, or Sn_xGa_y phases.[14,27] It can been seen from an enlarged view (Fig. 1b) of the peaks' position at about 38° that the peaks are located at 38.27°, 38.19°, 38.12°, and 37.92° for x equal to 0, 0.2, 0.6, and 1.0, respectively, indicating the peaks' position moves to smaller 2θ gradually with the increase of Sn content. The moved peaks' position is attributed to an increase in the lattice constants with the increase of Sn content (Ga^{3+} and Sn^{4+} ionic radii are 0.62 Å and 0.69 Å, respectively).[15,28,29] Based on the

powder diffraction file, the peaks' position of about 19°, 38°, and 59° is corresponding to ($\bar{2}01$), ($\bar{4}02$), and ($\bar{6}03$) of monoclinic β-phase Ga_2O_3, respectively (PDF# 43-1012). The full width at half maximum (FWHM) of the peaks increases for x = 0.6 and 1.0 (Fig. 1c), which reveals the serious decline of the crystalline quality of thin films. The radius of Sn^{4+} is bigger than that of Ga^{3+}, the order of the β-phase lattice is affected with the Ga^{3+} ions replaced by too many Sn^{4+} ions, leading to aGa_2O_3 lattice being destroyed. The clear and stripy RHEED patterns of β-phase $Ga_{2-x}Sn_xO_3$ (x = 0, 0.2) thin films are shown by the inset to Fig. 1a, indicating that the thin films are of single phase with very flat and smooth surfaces. Figure 1c also shows the relationship between ($\bar{4}02$) plane distance and Sn content; the spacing d is almost linear with increases in Sn content x.

Figure 2a shows the optical absorption spectrums of the β-phase $Ga_{2-x}Sn_xO_3$ thin films with different Sn content. The absorption coefficient of $Ga_{2-x}Sn_xO_3$ thin films obviously increases with the increase of Sn content at the same wavelength. The E_g of thin films can be derived according to the energy exponential relation[30]:

$$\alpha h\nu = B(h\nu - E_g)^n, \quad (1)$$

where α is the absorption coefficient, $h\nu$ is the energy of the incident photon, B is the constant, and the exponent n is equal to 0.5 for direct transitions, respectively. The E_g of thin films is obtained through fitting the linear region of the $(\alpha h\nu)^2$ versus $h\nu$ plot showing by the inset to Fig. 2a. The E_g is 4.97 eV, 4.86 eV, 4.52 eV, and 4.24 eV for x equal to 0, 0.2, 0.6 and 1.0, respectively, and Sn content x is almost equal to the measured value by EDX spectrum (not shown). Figure 2b depicts the pattern of a linear relationship between E_g and Sn content, and the E_g is fitted with a linear relationship equation[31] as follows:

$$E_g(Ga_{2-x}Sn_xO_3) = (1 - x/2)E_g(Ga_2O_3) + (x/2)E_g(SnO_2). \quad (2)$$

The decrease of the $E_{g\ that}$ can be ascribed to the narrower E_g of SnO_2 is 3.6 eV,[32] which is lower than that of β-phase Ga_2O_3.[33] Due to the E_g corresponding to the cut-off wavelength, we could adjust the cut-off wavelength from 249 nm ($E_g \sim 4.97$ eV) to 292 nm ($E_g \sim 4.24$ eV) through increasing Sn content. The modulation of the E_g through controlling Sn content also offers an efficient way toward the development of the longer wavelength UV PDs.

The top-view FE-SEM images of β-phase $Ga_{2-x}Sn_xO_3$ (x = 0, 0.2) thin films, which have fine crystalline quality, are exhibited in Fig. 3a and b. The $Ga_{2-x}Sn_xO_3$ (x = 0.2) thin film obviously has a relatively smooth and flat surface, and there are some cracks or pits on the surface of the $Ga_{2-x}Sn_xO_3$ (x = 0) thin film. Figure 3c and d show the cross-sectional images of $Ga_{2-x}Sn_xO_3$ (x = 0, 0.2) thin films; the interface between substrate and thin film can be observed. The heteroepitaxy grown film is compact, and the interface is flat for the $Ga_{2-x}Sn_xO_3$ (x = 0.2) thin film, indicating that the lattice mismatch ratio decreases between β-phase Ga_2O_3 and Al_2O_3 through doping SnO_2. This characteristic is beneficial for stable and reliable device operation. The thicknesses of the two thin films are all about 250 nm, corresponding to a growth rate of 0.28 Å/pulse. The EDX spectrum indicates that the film surfaces contain only Ga, O and Ga, Sn, O, indicating no impurities contamination during the deposition process.

The thin films for x = 0, 0.2, which have fine crystalline quality, are chosen as the PD and the schematic illustration is shown in Fig. 4a. A four-pair interdigital electrode is deposited on the surface of the thin film through a shadow mask for detecting the UV photoresponse. The UV-lamp with the wavelength of 254 nm is illuminated on the fabricated PD with an effective irradiated area of ~0.045 cm^2. Figure 4b and c show the measured I-V characteristic curves of β-phase $Ga_{2-x}Sn_xO_3$ PDs with x = 0, 0.2, respectively. It can be seen that the current linear response increases with the increases of bias voltage both under different illumination

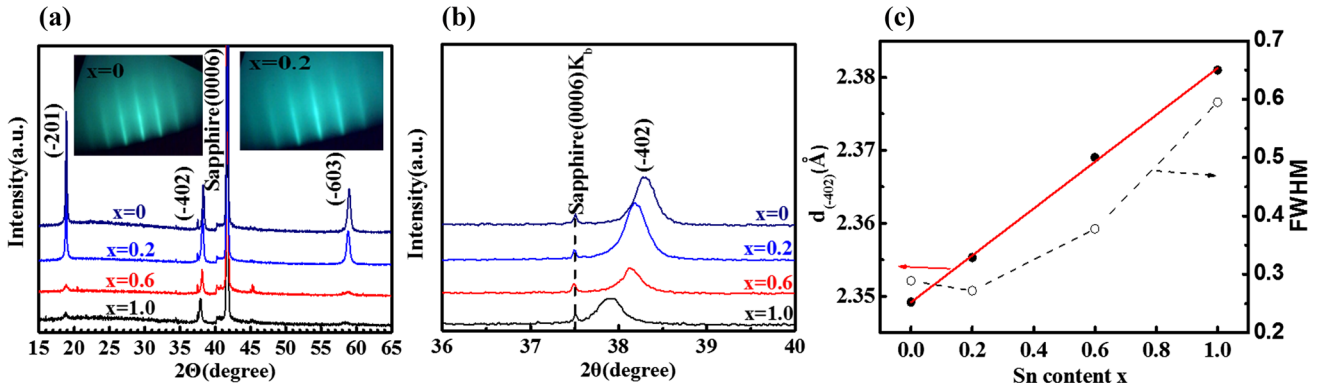

Fig. 1. (a) XRD patterns of the β-phase $Ga_{2-x}Sn_xO_3$ films with different Sn content x and the RHEED patterns of β-phase $Ga_{2-x}Sn_xO_3$ (x = 0, 0.2) films (insert). (b) Enlarged view of the peaks' position at about 38°. (c) Plot of both ($\bar{4}02$) plane distance and FWHM versus Sn content x.

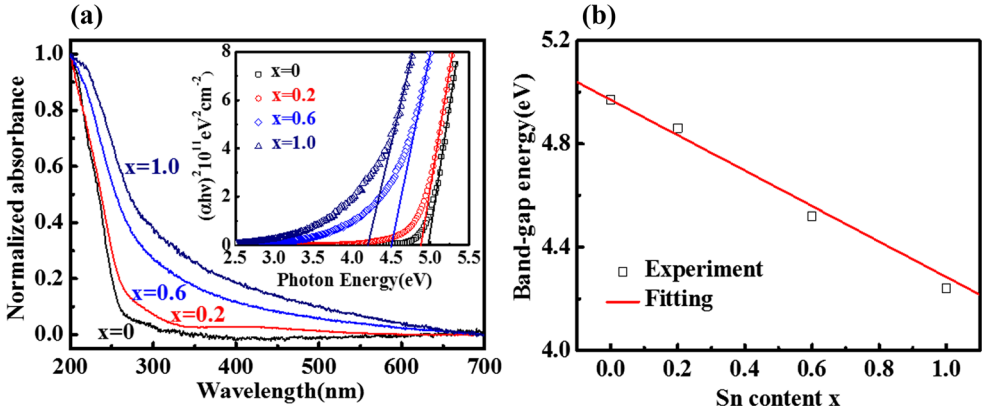

Fig. 2. (a) Absorption spectrums of β-phase $Ga_{2-x}Sn_xO_3$ thin films with different Sn content x, the E_g can be derived by fitting the linear region of the $(\alpha h\nu)^2$ versus $h\nu$ plot shown by the inset. (b) Plot of E_g versus Sn content x.

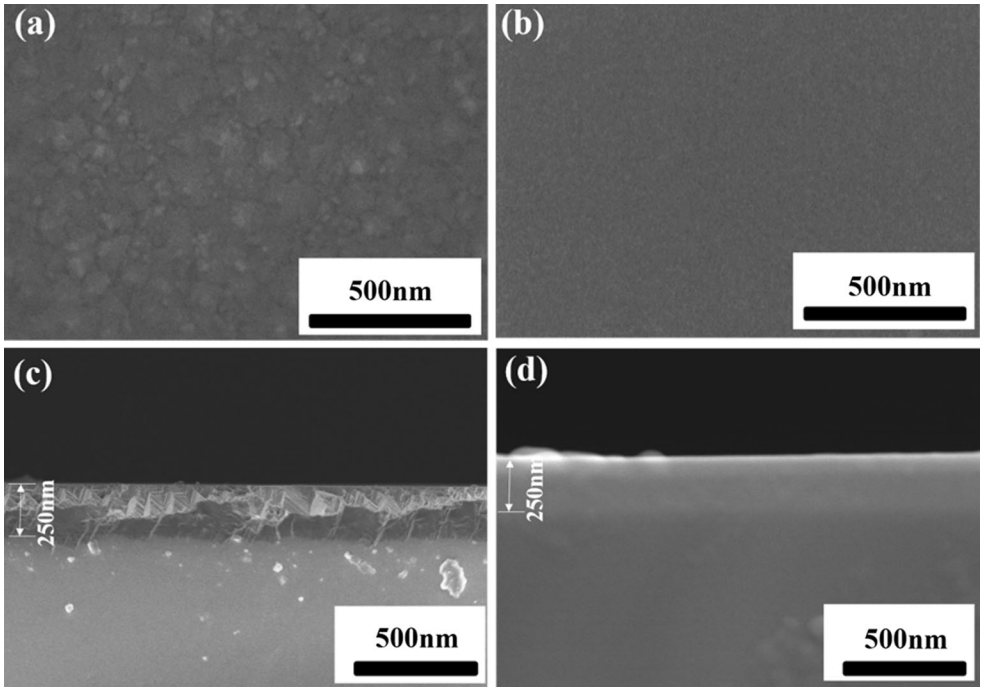

Fig. 3. Top-view FE-SEM images of (a) β-phase Ga_2O_3 thin film and (b) β-phase $Ga_{1.8}Sn_{0.2}O_3$ thin film, cross-sectional FE-SEM images of (c) β-phase Ga_2O_3 thin film and (d) β-phase $Ga_{1.8}Sn_{0.2}O_3$ thin film.

conditions and in the dark, indicating that a good ohmic contact has formed between Au/Ti electrode and thin films. The measured I-V curve in the dark shows the dark current of $Ga_{2-x}Sn_xO_3$ (x = 0.2) thin film is slightly more than $Ga_{2-x}Sn_xO_3$ (x = 0) at the same bias voltage, and there is a more significant increase in the photocurrent to $Ga_{2-x}Sn_xO_3$ (x = 0.2) thin film when illuminating with the 254 nm UV light. Figure 4d shows the responsivity of two PDs under different illumination conditions, calculated by:

$$R = (I_{\text{light}} - I_{\text{dark}})/(P \cdot S), \tag{3}$$

where R is the responsivity of irradiation, I_{light}, I_{dark} represent the light current and the dark current, P is the irradiation power density, and S is the effective area of PD, respectively. The responsivity of $Ga_{2-x}Sn_xO_3$ (x = 0.2) PD is 3.61×10^{-2} A/W under 254 nm UV illumination (140 μW/cm^2) at 50 V, and it almost increases by one order of magnitude greater than that of $Ga_{2-x}Sn_xO_3$ (x = 0) PD. Increases in current intensity and responsivity are caused by the increase of conductivity, the Ga^{3+} ions located in the lattice are replaced by Sn^{4+} ions or the Sn^{4+} ions themselves will act as interstitial atoms, both of which play the role of donor and cause an increase in conduction electrons. Meanwhile, the ionic radii difference between Sn^{4+} ions ($\sim$ 0.69 Å) and Ga^{3+} ions ($\sim$0.62 Å) would result in a slight lattice expansion and enhanced carrier

mobility. In addition, a decrease in (E_g) is beneficial to the interband transition of the carrier.

Figure 5a and b exhibit the time-dependent photoresponse of β-phase $Ga_{2-x}Sn_xO_3$ (x = 0, 0.2) PDs to 254 nm illumination with different optical input power by on/off switching at 50 V. To the β-phase $Ga_{2-x}Sn_xO_3$ (x = 0) PD, the current of around 1 nA in the dark increases to 23.89 nA, 27.04 nA, and 35.66 nA for incident optical power of 80 μW/cm^2, 100 μW/cm^2 and 140 μW/cm^2, respectively. However, the current increases instantaneously from about 10 nA to 121.09 nA, 148.18 nA and 205.70 nA with incident optical power of 80 μW/cm^2, 100 μW/cm^2 and 140 μW/cm^2 for β-phase $Ga_{2-x}Sn_xO_3$ (x = 0.2) PD. The photocurrent almost linearly increases with increasing optical input power. The photoresponse process of β-phase $Ga_{2-x}Sn_xO_3$ (x = 0, 0.2) PDs under 254 nm illumination (140 μW/cm^2) is well fitted with a bi-exponential relaxation equation as shown in Fig. 5c and d, and the bi-exponential relaxation equation[14,33] is as follows:

$$I = I_0 + Ae^{-t/\tau 1} + Be^{-t/\tau 2}, \quad (4)$$

where I_0 is the steady state current, A and B are two constants, t is the time, and τ is the relaxation time constant, respectively. τ_r and τ_d represent the relaxation time constants for the rising edge and falling edge in Fig. 5c and d. The τ_{r1} and τ_{r2} of two PDs are estimated to be 1.04 s/13.92 s and 0.94 s/10.04 s, and the τ_d is estimated to be 12.13 s and 1.37 s, respectively. To the τ_r, the fast-response component is caused by the rapid change of the carrier concentration as soon as the light is turned on/off, and the slow-response component is attributed to the carrier trapping/releasing owing to the existence of oxygen vacancy defects in thin films. The carriers captured by the trapping states would be released and generated. Usually, the traps in a wide E_g semiconductor are extremely deep.[34] The time constant of the transient decay is governed by the depth of these traps and can be very long. In our case, the presence of numerous trapping states prevents carriers' generation that may cause the slow recovery time.[35] In addition, a decrease in the relaxation time constants for x = 0.2 is ascribed to an increase in the carrier and interband transition easily done with the narrower E_g.

Table I shows the characteristic parameters of the two PDs under different illumination conditions at 50 V. Generally, the PD exhibits an excellent SB UV characteristic with higher responsivity and shorter relaxation time constants for the $Ga_{2-x}Sn_xO_3$ (x = 0.2) thin film. The responsivity is 6.41 × 10^{-3} A/W for $Ga_{2-x}Sn_xO_3$ (x = 0) thin film, and increases to 3.61 × 10^{-2} A/W for $Ga_{2-x}Sn_xO_3$ (x = 0.2) thin film under 254 nm UV illumination (140 μW/cm^2) at 50 V. Both τ_r and τ_d of $Ga_{2-x}Sn_xO_3$ (x = 0.2) thin film are estimated to be 1.33 s/14.05 s,

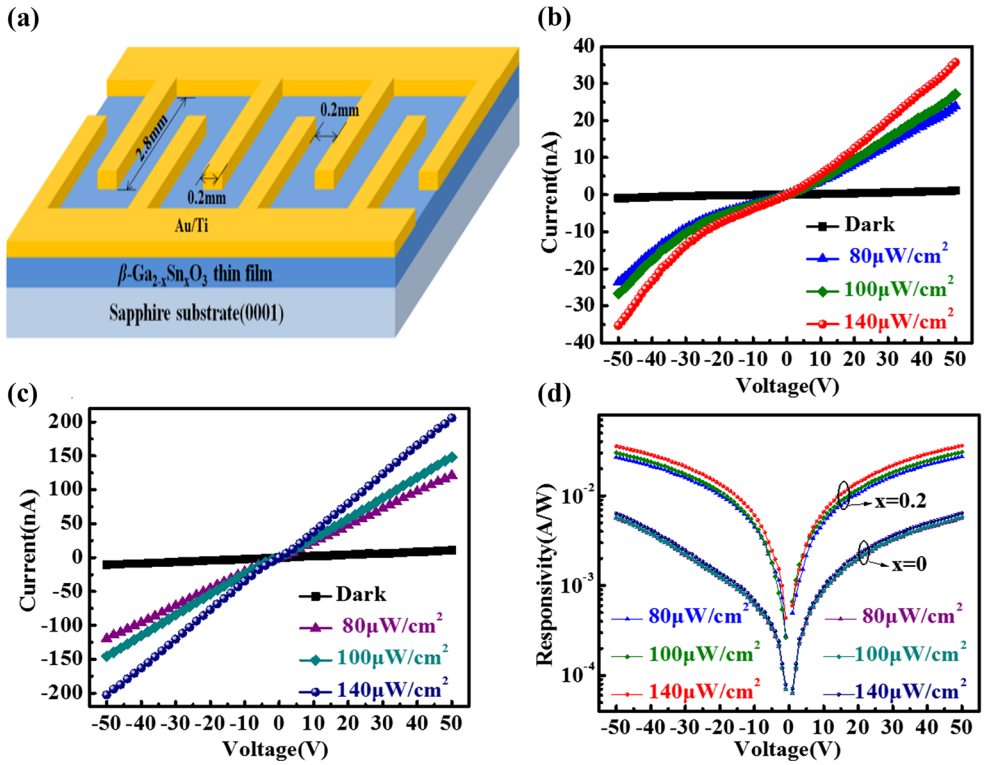

Fig. 4. (a) Schematic illustration of β-phase $Ga_{2-x}Sn_xO_3$ PD. I-V characteristic curves of (b) β-phase Ga_2O_3 PD and (c) β-phase $Ga_{1.8}Sn_{0.2}O_3$ PD. (d) Responsivity of two PDs under different illumination conditions.

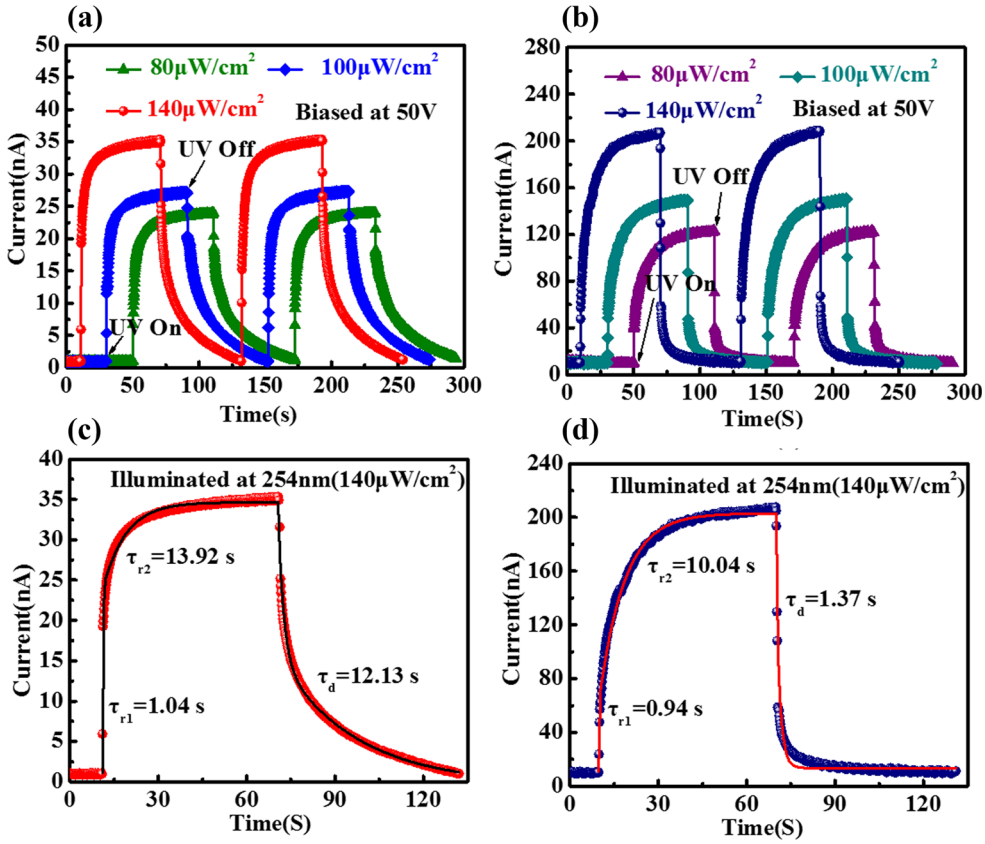

Fig. 5. Time-dependent photoresponse of (a) β-phase Ga_2O_3 PD and (b) β-phase $Ga_{1.8}Sn_{0.2}O_3$ PD, experimental and fitted curve of the current rising and decay process for (c) β-phase Ga_2O_3 PD and (d) β-phase $Ga_{1.8}Sn_{0.2}O_3$ PD.

Table I. The characteristic parameters of β-phase $Ga_{2-x}Sn_xO_3$ (x = 0, 0.2) PDs under different illumination conditions (All the measurements are at 50 V)

Items	Ga_2O_3	$Ga_{1.8}Sn_{0.2}O_3$
Current (nA)[Dark]	1.04	10.79
Current (nA)[80 μW/cm^2]	23.89	121.09
Current (nA)[100 μW/cm^2]	27.04	148.18
Current (nA)[140 μW/cm^2]	35.66	205.70
Responsivity(A/W) [80 μW/cm^2]	5.64×10^{-3}	2.72×10^{-2}
Responsivity(A/W) [100 μW/cm^2]	5.78×10^{-3}	3.05×10^{-2}
Responsivity(A/W) [140 μW/cm^2]	6.41×10^{-3}	3.61×10^{-2}
τ_{r1}/τ_{r2} (s) [80 μW/cm^2]	1.50/15.86	1.33/14.05
τ_{r1}/τ_{r2} (s) [100 μW/cm^2]	1.42/14.02	1.03/12.46
τ_{r1}/τ_{r2} (s) [140 μW/cm^2]	1.04/13.92	0.94/10.04
τ_d (s) [80 μW/cm^2]	15.90	3.17
τ_d (s) [100 μW/cm^2]	15.71	2.71
τ_d (s) [140 μW/cm^2]	12.13	1.37

3.17 s; 1.03 s/12.46 s, 2.71 s and 0.94 s/10.04 s, 1.37 s for the incident optical power of 80 μW/cm^2, 100 μW/cm^2 and 140 μW/cm^2, respectively, which is shorter than that of $Ga_{2-x}Sn_xO_3$ (x = 0) thin film. These results suggest the performance of SBPD could be improved by doping Sn^{4+} in Ga_2O_3 thin films.

CONCLUSIONS

($\bar{2}$01) oriented β-phase $Ga_{2-x}Sn_xO_3$ thin films were grown on Al_2O_3 (0001) substrates with different Sn content. The crystal lattice expands, and the energy band-gap decreases with the increase of Sn content. The n-type conductivity generates by doping Sn^{4+} ions in Ga_2O_3 thin films in the oxygen-poor

conditions. The SBPD with a MSM structure based on β-phase $Ga_{2-x}Sn_xO_3$ ($x = 0.2$) thin film shows excellent SB UV characteristics with higher responsivity and shorter relaxation time constants under 254 nm UV light irradiation. The results suggest a potential application in SBPD for Sn-doped Ga_2O_3 thin films.

ACKNOWLEDGEMENTS

This work was supported by the National Natural Science Foundation of China (Nos. 51572033, 11404029, 51172208), Beijing Natural Science Foundation (No. 2154055), the Beijing University of Posts and Telecommunications (BUPT) Excellent Ph.D. Students Foundation (CX2015304), and the China Postdoctoral Science Foundation Funded Project (Grant No. 2014M550661).

REFERENCES

1. A. Malik, A. Sêco, E. Fortunato, and R. Martins, *Sens. Actuators A* 67, 68 (1998).
2. L. Li, E. Auer, M. Liao, X. Fang, T. Zhai, U.K. Gautam, A. Lugstein, Y. Koide, Y. Bando, and D. Golberg, *Nanoscale* 3, 1120 (2011).
3. N. Biyikli, I. Kimukin, T. Kartaloglu, O. Aytur, and E. Ozbay, *Appl. Phys. Lett.* 82, 2344 (2003).
4. K. Nomura, H. Ohta, K. Ueda, T. Kamiya, M. Hirano, and H. Hosono, *Science* 300, 1269 (2003).
5. W.Y. Weng, T.J. Hsueh, S.J. Chang, G.J. Huang, H.T. Hsueh, Z.D. Huang, and C.J. Chiu, *IEEE Sens. J.* 11, 1795 (2011).
6. M. Liao, Y. Koide, and J. Alvarez, *Appl. Phys. Lett.* 87, 022105 (2005).
7. X. Du, Z. Mei, Z. Liu, Y. Guo, T. Zhang, Y. Hou, Z. Zhang, Q. Xue, and A.Y. Kuznetsov, *Adv. Mater.* 21, 4625 (2009).
8. R. Roy, V.G. Hill, and E.F. Osborn, *J. Am. Chem. Soc.* 74, 719 (1952).
9. M. Passlack, E.F. Schubert, W.S. Hobson, M. Hong, N. Moriya, S.N.G. Chu, K. Konstadinidis, J.P. Mannaerts, M.L. Schnoes, and G.J. Zydzik, *J. Appl. Phys.* 77, 686 (1995).
10. G.A. Battiston, R. Gerbasi, M. Porchia, R. Bertoncello, and F. Caccavale, *Thin Solid Films* 279, 115 (1996).
11. S. Geller, *J. Chem. Phys.* 33, 676 (1960).
12. H. Aida, K. Nishiguchi, H. Takeda, N. Aota, K. Sunakawa, and Y. Yaguchi, *Jpn. J. Appl. Phys.* 47, 8506 (2008).
13. W.Y. Weng, T.J. Hsueh, S.J. Chang, G.J. Huang, and H.T. Hsueh, *IEEE Sens. J.* 11, 999 (2011).
14. D.Y. Guo, Z.P. Wu, P.G. Li, Y.H. An, H. Liu, X.C. Guo, H. Yan, G.F. Wang, C.L. Sun, L.H. Li, and W.H. Tang, *Opt. Mater. Express.* 4, 1067 (2014).
15. Y. Kokubun, K. Miura, F. Endo, and S. Nakagomi, *Appl. Phys. Lett.* 90, 031912 (2007).
16. D.Y. Guo, Z.P. Wu, Y.H. An, X.C. Guo, X.L. Chu, C.L. Sun, L.H. Li, P.G. Li, and W.H. Tang, *Appl. Phys. Lett.* 105, 023507 (2014).
17. X.L. Zhao, Z.P. Wu, W. Cui, Y.S. Zhi, D.Y. Guo, L.H. Li, W.H. Tang, *ACS Appl. Mater. Interfaces*. 9, 983 (2017).
18. N. Ueda, H. Hosono, R. Waseda, and H. Kawazoe, *Appl. Phys. Lett.* 70, 3561 (1997).
19. Z. Hajnal, J. Miro, G. Kiss, F. Reti, P. Deak, R.C. Herndon, and J.M. Kuperberg, *J. Appl. Phys.* 86, 3792 (1999).
20. M. Orita, H. Ohta, M. Hirano, and H. Hosono, *Appl. Phys. Lett.* 77, 4166 (2000).
21. M.D. Heinemann, J. Berry, G. Teeter, T. Unold, and D. Ginley, *Appl. Phys. Lett.* 108, 022107 (2016).
22. X.J. Du, Z. Li, C.N. Luan, W.G. Wang, M.X. Wang, X.J. Feng, H.D. Xiao, and J. Ma, *J. Mater. Sci.* 50, 3252 (2015).
23. W. Mi, X.J. Du, C.N. Luan, H.D. Xiao, and J. Ma, *RSC Adv.* 4, 30579 (2014).
24. W. Mi, Z. Li, C.N. Luan, H.D. Xiao, C.S. Zhao, and J. Ma, *Ceram. Int.* 41, 2572 (2015).
25. J. Kudou, S. Funasaki, M. Takahara, I. Tsunoda, K. Takakura, H. Ohyama, T. Nakashima, M. Shibuya, K. Murakami, E. Simoen, and C. Claeys, *Mater. Sci. Forum* 725, 269 (2012).
26. D.Y. Guo, X.L. Zhao, Y.S. Zhi, W. Cui, Y.Q. Huang, Y.H. An, P.G. Li, Z.P. Wu, and W.H. Tang, *Mater. Lett.* 164, 364 (2016).
27. Joint Committee on Powder Diffraction Standards (JCPDS), Powder Diffraction Files, Inorganic, No. 43-1012.
28. X.L. Zhao, Z.P. Wu, D.Y. Guo, W. Cui, P.G. Li, Y.H. An, L.H. Li, and W.H. Tang, *Semicond. Sci. Technol.* 31, 6 (2016).
29. D.Y. Guo, Y.H. An, W. Cui, X.L. Zhao, Y.S. Zhi, M. Lei, L.H. Li, P.G. Li, Z.P. Wu, and W.H. Tang, *Sci. Rep.* 6, 25166 (2016).
30. J. Tauc and F. Abeles, *Optical Properties of Solids* (Amsterdam: North Holland, 1972).
31. I. Vurgaftman, J.R. Meyer, and L.R. Ram-Mohan, *J. Appl. Phys.* 89, 5815 (2001).
32. Z. Liu, D. Zhang, S. Han, C. Li, and T. Tang, *Adv. Mater.* 15, 1754 (2003).
33. N. Liu, G. Fang, W. Zeng, H. Zhou, F. Cheng, Q. Zheng, L. Yuan, X. Zou, and X. Zhao, *ACS. Appl. Mater. Int.* 2, 1973 (2010).
34. T. Murphy, K. Moazzami, and J. Phillips, *J. Electron. Mater.* 35, 543 (2006).
35. P. Ravadgar, R.H. Horng, S.D. Yao, H.Y. Lee, B.R. Wu, S.L. Ou, and L.W. Tu, *Opt. Express* 21, 24599 (2013).